Appl Compos Mater (2017) 24:625–642
DOI 10.1007/s10443-016-9531-2

Effect of Nesting on the Permeability of Multilayer Unidirectional Fabrics

Jianjun Jiang[1] · **Yang Su**[1] · **Linchao Zhou**[1] · **Qiang Guo**[1] · **Chumeng Xu**[1] · **Guoli Deng**[1] · **Xing Chen**[1] · **Xuming Yao**[1] · **Liangchao Fang**[1]

Received: 5 September 2016 / Accepted: 8 September 2016 / Published online: 10 October 2016

Abstract Nesting of layers is the main source of the variations in permeability values in liquid composite molding (LCM) processes. In this paper, the permeability of unidirectional fabrics was modeled as a function of layer shift and geometrical yarn parameters to study the effect of nesting. Firstly, three different unit cells of two layers were modeled based on the range of layer shift and decomposed into zones of characteristic yarn arrangement, respectively. The overall permeability of each unit cell was then modeled as a mixture of local permeabilities of different zones with the electrical resistance analogy. Secondly, every two adjacent layers were regarded as porous media with different permeabilities. The permeability of multilayer unidirectional fabrics was then modeled with electrical resistance analogy. As the unpredictability of layer shifting in actual process, the statistical characteristics were analyzed theoretically and validated with experimental measurements. Excellent agreement was found between predictions and experiment data.

Keywords Fabrics · Permeability · Analytical modelling · Liquid composite moulding

1 Introduction

Advanced polymer matrix composites have been widely used in aerospace, marine, and automotive industries [1–4], due to the excellent mechanical properties include high specific strength, high specific stiffness and excellent fatigue performance, etc. But the development is restricted by the high cost of the composite manufacturing. Liquid composite molding (LCM)

✉ Jianjun Jiang
jianjun@nwpu.edu.cn

[1] Shaanxi Engineering Research Center for Digital Manufacturing Technology, Northwestern Polytechnical University, Xi'an 710072, People's Republic of China

processes have become one of mainstream technologies to realize low-cost. In the process, the reinforcement are placed and held stationary by compacting them in a mold cavity and a thermoset resin is injected into the mold to cover the empty spaces between the fibers [5, 6]. The permeability of the fiber preform, which represents the resistance of flowing through a porous medium, is an important parameter influencing the resin impregnation process. Therefore, the characterization of preform permeability is a key issue to optimize process parameters and establish the optimum process window for manufacturing processes to fabricate high-quality products [7–9].

Nesting related to layer shift is a geometric phenomenon and inevitably occurs during the process of ply stacking. It generally refers to (partial) filling of inter-yarn voids on the surface of a layer by yarns of an adjacent layer. The nesting of adjacent layers can largely change the flow path and it is one of the main sources of the observed scatter in permeability experiments [10]. Dungan et al. [11] and Senogus et al. [12] demonstrated that the permeability values could differ by a decimal order of magnitude for zero- and maximum nesting configurations of the laminate. Endruweit et al. [13, 14] found that the effect of nesting contributed significantly to the permeability variations. To predict the permeability of textiles with nesting, Grujicic et al. [15, 16] and Lekakou et al. [17] developed numerical models. However, the limitation of numerical calculations is that a particular effort is required to solve Navier-Stokes equations on a very delimited domain that unit cell has to be constructed in terms of geometry and mesh [18].

In our previous works, analytical models were established to study the nesting on in-plane and out-of-plane permeability of unidirectional fabrics [19, 20]. But these models are applied only to a two-layer fabric with minimum nesting or maximum nesting. Besides, the layer shift must be given in advance to predict the permeability. For multilayer fabrics, the shifting between adjacent layers is independent and random. The layer shift is difficult to obtain in actual process. The method that could predict the permeability of multilayer fabric without being given the layer shift values has great guiding significance for practical engineering application. Zeng et al. [21] made an attempt to consider the effect of random layer shift in numerical permeability analysis of multilayer woven fabrics. To possess a comprehensive understanding, the analytical modeling is worth performing.

In this article, the effect of nesting on the permeability of unidirectional fabrics was investigated experimentally and theoretically. Firstly, analytical models of the permeability of a two-layer fabric correlated with geometrical yarn parameters were built with the electrical resistance analogy. The fabric permeability was associated with average thickness per layer, fabric structure and layer shifting, so the models can be used to describe the permeability of fabrics not only with extreme nesting (minimum or maximum nesting) but also with random nesting. Secondly, based on the model of a two-layer fabric, statistical analysis on the permeability of multilayer fabrics was carried out to provide insight into how permeability varies with respect to the number of layers and layer shift. With the theoretical model, the distribution of permeability for multilayer fabrics can be predicted without being given the layer shift values.

2 Theoretical Modeling

For unidirectional multilayer fabrics, nesting is characterized by arrangement of the yarn throughout the laminate by shifting each layer in x direction (Fig. 1). Assuming that the

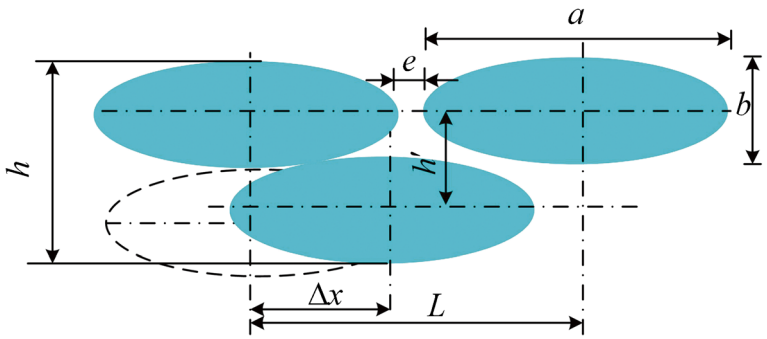

Fig. 1 Schematic of nesting between adjacent layers for unidirectional fabrics

periodicity of layers is perfect, the average layer thickness which is defined as the overall thickness divided by the number of layers can be estimated as

$$\overline{h} = \frac{(n-1)h'}{n} \text{ or } \overline{h} = b\left[\left(1-\frac{1}{n}\right)\sqrt{1-\left(\frac{\Delta x}{a}\right)^2}+\frac{1}{n}\right] \quad 0 \le \Delta x \le L/2 \tag{1}$$

where h' is the distance between adjacent layers. Δx is the horizontal translation in x-direction. a and b are long and short axes of the tow cross-section, respectively. n is the number of layers. L is the horizontal distance between adjacent ellipse centers.

There are three different ply stacking sequences: (1) Zero nesting: the pores align in through-thickness direction along the different layers, and $\overline{h} = b$ when $\Delta x = 0$; (2) Maximum nesting: the gaps between yarns of a layer are partially filled with fiber bundles of an adjacent layer. This effect can occur even if the inter-yarn gaps are closed. In this case, the average layer thickness is minimum when $\Delta x = L/2$; (3) Partial nesting: no special attention is spent on the relative position of the layers and this case lies between zero nesting and maximum nesting when $0 < \Delta x < L/2$.

2.1 Two-Layer Fabric

Because of the yarn cross-sectional shapes, the geometry of the voids between adjacent yarns is complex, and there is no analytical solution for their influence on the layer permeability. It is estimated based on the simplified geometry illustrated in Fig. 2. The cross section of the fiber bundle is simplified from an ellipse to a rectangle. The total cross-sectional area of voids is represented by two rectangular gaps with height $\Delta w/2$ and width a.

$$\Delta w = \left(1-\frac{\pi}{4}\right)b \tag{2}$$

The gap can be characterized approximately by the equivalent permeability from the analytical solution to the Poiseuille duct flow [22]:

$$K_{gap,x} = K_{gap,y} = f_c \frac{8(\Delta w/2)^2}{a\pi^4}\left(a + \frac{(\cosh(\pi a/(\Delta w/2))-1)^2-\sinh^2(\pi a/(\Delta w/2))}{(\pi/(\Delta w/2))\sinh^2(\pi a/(\Delta w/2))}\right) \tag{3}$$

where f_c is the correction factor to describe the gap geometry and is related to the hydraulic diameter, which describes the ratio between the gap cross-sectional area and perimeter. The correction factor f_c introduced here describes the gap geometry and is related to the hydraulic

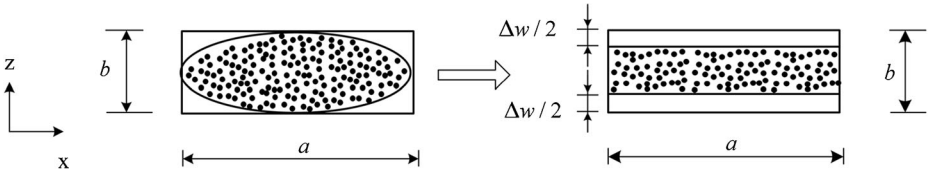

Fig. 2 Yarn cross-section and bounding box; simplification of void geometry

diameter, which describes the ratio between the gap cross-sectional area and perimeter. As Endruwei et al. [14] suggested, the value of f_c is smaller than 1, since the ratio of cross-sectional area and perimeter is smaller for a duct enclosed by a rectangle and two semi-ellipses than for a rectangular duct with equivalent cross-sectional area. Here f_c is estimated as the ratio of hydraulic diameters before and after simplification, written as follows:

$$f_c = \frac{A_{bef} C_{aft}}{A_{aft} C_{bef}} \tag{4}$$

where A_{bef} and A_{aft} are the cross-sectional areas before and after simplification, respectively. C_{bef} and C_{aft} are the perimeters before and after simplification, respectively.

For the permeability of the yarn, equations proposed by Gebart [23], are used:

$$K_{yarn\parallel} = 8r_f^2(1-V_b)^3/\left(C_\parallel V_b^2\right) \tag{5}$$

$$K_{yarn\perp} = C_\perp r_f^2\left(\sqrt{V_{b,\max}/V_b}-1\right)^{5/2} \tag{6}$$

where $K_{yarn\parallel}$ and $K_{yarn\perp}$ are the permeabilities of the flow along and perpendicular to the filament axis, respectively. r_f is the radius of fiber filament. V_b is the fiber volume fraction of a fiber bundle. $C_\parallel$, $C_\perp$ and $V_{b,\max}$ are constants for the two types of fiber arrangement summarized in Table 1.

For each bounding box as in Fig. 2, the liquid flows through the gaps and the yarn at the same time in x and y direction, therefore the flow resistances (equivalent to 1/K) are in parallel. In z direction, the liquid flows through the gaps and the yarn in succession, so the flow resistances (equivalent to 1/K) of the three regions are in series. With the electrical resistance analogy, the permeability values of bounding box can be estimated by

$$K_{box,x} = K_{gap,x}\frac{\Delta w}{b} + K_{yarn\perp}\frac{b-\Delta w}{b} \tag{7}$$

$$K_{box,y} = K_{gap,y}\frac{\Delta w}{b} + K_{yarn\parallel}\frac{b-\Delta w}{b} \tag{8}$$

$$K_{box,z} = \left(\frac{1}{K_{gap,z}}\frac{\Delta w}{b} + \frac{1}{K_{yarn\perp}}\frac{b-\Delta w}{b}\right)^{-1} \tag{9}$$

Table 1 Parameter values of permeability Eqs. (5) and (6)

Fiber arrangement	$C_\parallel$	$C_\perp$	$V_{b,\max}$
Quadratic	57	$\frac{16}{9\pi\sqrt{2}}$	$\frac{\pi}{4}$
Hexagonal	53	$\frac{16}{9\pi\sqrt{6}}$	$\frac{\pi}{2\sqrt{3}}$

As the permeability value of gaps is several orders higher than that of yarn in z direction, Eq. (10) can be rewriten as

$$K_{box,z} \approx K_{yarn\perp} \frac{b}{b-\Delta w} \tag{10}$$

A representative unit cell for a two-layer unidirectional fabric is shown in Fig. 3. Notice that the architecture of unit cell changes with respect to layer shift. According to the range of layer shift, three different unit cells are modeled. Due to the specific characteristic of two-scale porosity, we divide the unit cell into five different zones. The permeability of the unit cell can be modeled as a mixture of permeabilities of different zones with the electrical resistance analogy. In x direction, the liquid flows through the five different zones in succession, so the flow resistances are in series. In y and z directions, the liquid flows through the local regions at the same time, therefore the flow resistances are in parallel. Then the permeability of the unit cell can be estimated as:

$$K_x = \left(\sum_{i=1}^{5} \frac{1}{K_x^i} \frac{t_i}{a+e} \right)^{-1} \tag{11}$$

$$K_y = \sum_{i=1}^{5} K_y^i \frac{t_i}{a+e} \tag{12}$$

$$K_z = \sum_{i=1}^{5} K_z^i \frac{t_i}{a+e} \tag{13}$$

Where e is the width of gaps between yarns. t_i is the length of the zone i in x direction. K_x^i, K_y^i and K_z^i are permeabilities of the zone i in x, y and z directions, respectively. From Eqs. (11)–(13), it can be seen that the permeability of the unit cell with different shift ranges can be determined if the permeability of each zone is given.

For each zone in the decomposed unit cell, the local through-thickness fiber arrangements are approximated as illustrated in Figs. 3, 4, and 5. The effective local permeability of a zone can be estimated based on the permeability of the bounding box and the equivalent permeabilities of voids.

When $0 \le \Delta x \le e$, the arrangement of each zone of unit cell can be seen in Fig. 3. The fiber arrangement in zone 1 is the same with that in the bounding box. The permeabilities of zone 1 are

$$K_x^1 = K_{box,x} \tag{14}$$

$$K_y^1 = K_{box,y} \tag{15}$$

$$K_z^1 = K_{box,z} \tag{16}$$

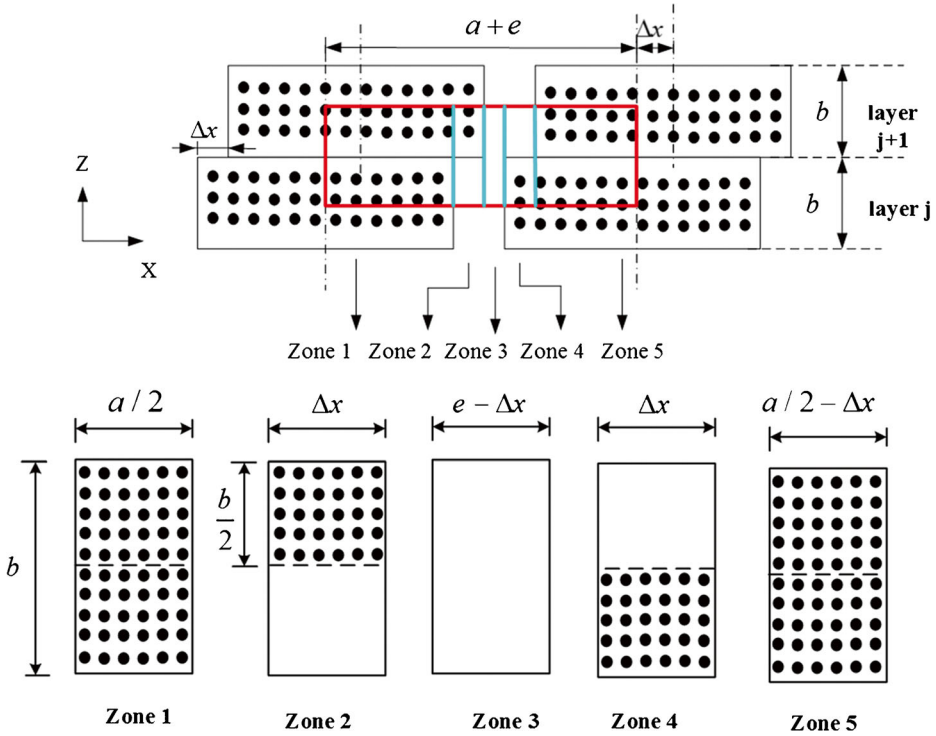

Fig. 3 Unit cell of unidirectional composites when $0 \le \Delta x \le e$, decomposed into five different zones

The zone 2 consists of two parts: the fiber region and the void space. The permeability of the fiber region is equal to the value of the bounding box. The equivalent permeability of the void space can also be obtained by:

$$K^2_{void,x} = K^2_{void,y} = \frac{(b/2)^2}{12} \tag{17}$$

$$K^2_{void,z} = \frac{(\Delta x)^2}{12} \tag{18}$$

With the electrical resistance analogy, the permeability of zone 2 can be estimated as:

$$K^2_x = \frac{1}{2} K_{box,x} + \frac{1}{2} K^2_{void,x} \tag{19}$$

$$K^2_y = \frac{1}{2} K_{box,y} + \frac{1}{2} K^2_{void,y} \tag{20}$$

$$K^2_z = \left(\frac{1}{2} \frac{1}{K_{box,z}} + \frac{1}{2} \frac{1}{K^2_{void,z}} \right)^{-1} \tag{21}$$

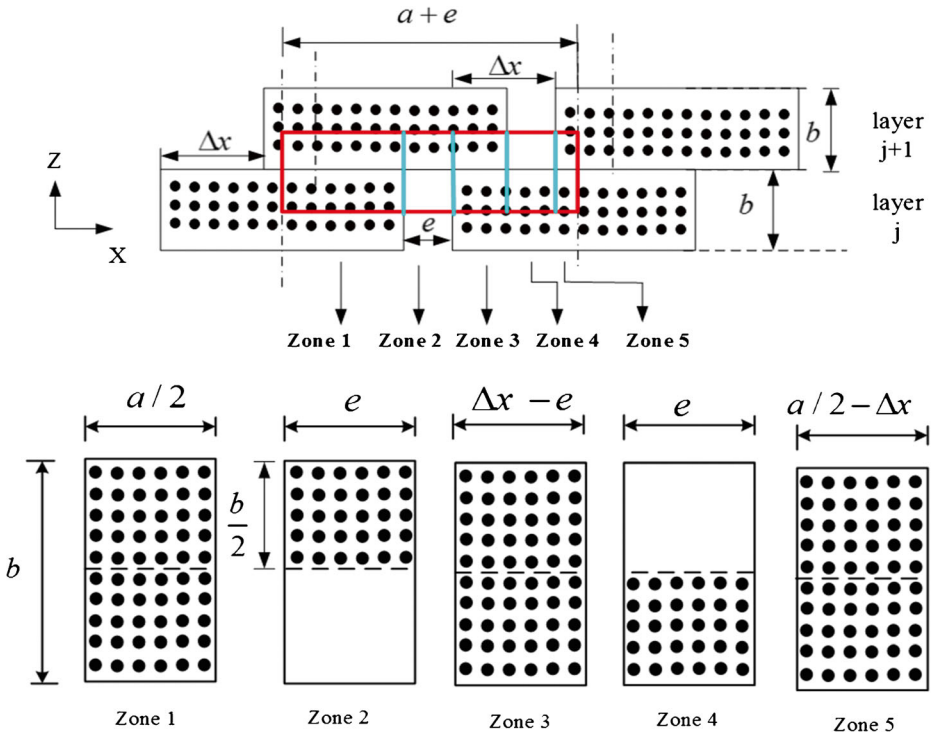

Fig. 4 Unit cell of unidirectional fabrics when $e \le \Delta x \le a/2$, decomposed into five different zones

The zone 3 contains no fiber and its equivalent permeability can be calculated as

$$K_x^3 = K_y^3 = \frac{b^2}{12} \tag{22}$$

$$K_z^3 = \frac{(e-\Delta x)^2}{12} \tag{23}$$

The fiber arrangement of zone 4 is similar with that of zone 2. Therefore,

$$K_x^4 = K_x^2 \tag{24}$$

$$K_y^4 = K_y^2 \tag{25}$$

$$K_z^4 = K_z^2 \tag{26}$$

The fiber arrangement of zone 5 is similar with that of bounding box. Therefore,

$$K_x^5 = K_{box,x} \tag{27}$$

$$K_y^5 = K_{box,y} \tag{28}$$

$$K_z^5 = K_{box,z} \tag{29}$$

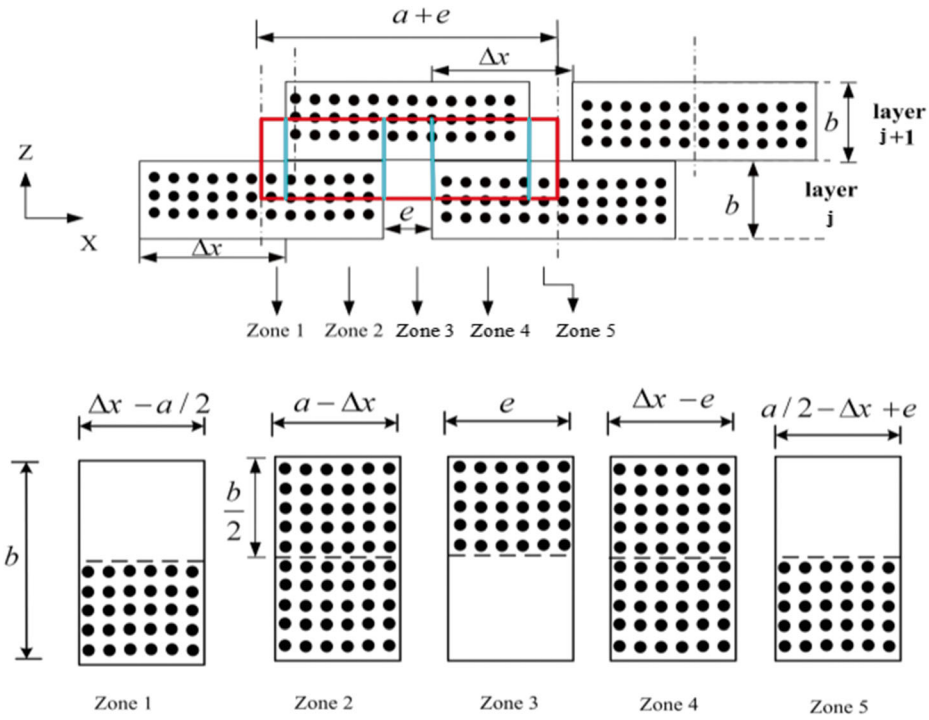

Fig. 5 Unit cell of unidirectional fabrics when $a/2 \le \Delta x \le L/2$, decomposed into five different zones

Substituting Eqs. (14)–(16), (19)–(29) into Eqs. (11)–(13), the in-plane and out-of-plane permeability of the unit cell can be obtained when $0 \le \Delta x \le e$.

When $e \le \Delta x \le a/2$, the arrangement of each zone of unit cell can be seen in Fig. 4. The equivalent permeability of the void space in zone 2 can also be obtained by:

$$K^2_{void,x} = K^2_{void,y} = \frac{(b/2)^2}{12} \tag{30}$$

$$K^2_{void,z} = \frac{e^2}{12} \tag{31}$$

With the electrical resistance analogy, the in-plane and out-of-plane permeabilities of each zone are listed in Table 2 when $e \le \Delta x \le a/2$.

When $a/2 \le \Delta x \le L/2$, the arrangement of each zone of unit cell can be seen in Fig. 5. The equivalent permeability of the void space in zone 1 can be obtained by:

$$K^1_{void,x} = K^1_{void,y} = \frac{(b/2)^2}{12} \tag{32}$$

$$K^1_{void,z} = \frac{(\Delta x - a/2)^2}{12} \tag{33}$$

Table 2 The permeability of each zone when $e \le \Delta x \le a/2$

Zone	Permeability		
	K_x	K_y	K_z
1	$K_x^1 = K_{box,x}$	$K_y^1 = K_{box,y}$	$K_z^1 = K_{box,z}$
2	$K_x^2 = \frac{1}{2}K_{box,x} + \frac{1}{2}K_{void,x}^2$	$K_y^2 = \frac{1}{2}K_{box,y} + \frac{1}{2}K_{void,y}^2$	$K_z^2 = \left(\frac{1}{2}\frac{1}{K_{box,z}} + \frac{1}{2}\frac{1}{K_{void,z}^2}\right)^{-1}$
3	$K_x^3 = K_{box,x}$	$K_y^3 = K_{box,y}$	$K_z^3 = K_{box,z}$
4	$K_x^4 = K_x^2$	$K_y^4 = K_y^2$	$K_z^4 = K_z^2$
5	$K_x^5 = K_{box,x}$	$K_y^5 = K_{box,y}$	$K_z^5 = K_{box,z}$

The equivalent permeability of the void space in zone 3 can be obtained by:

$$K_{void,x}^3 = K_{void,y}^3 = \frac{(b/2)^2}{12} \tag{34}$$

$$K_{void,z}^3 = \frac{e^2}{12} \tag{35}$$

The zone 5 consists of two parts: the fiber region and the void space. The equivalent permeability of the void space in zone 5 can be obtained by:

$$K_{void,x}^5 = K_{void,y}^5 = \frac{(b/2)^2}{12} \tag{36}$$

$$K_{void,z}^5 = \frac{(a/2 - \Delta x + e)^2}{12} \tag{37}$$

With the electrical resistance analogy, the in-plane and out-of-plane permeabilities of each zone are listed in Table 3 when $a/2 \le \Delta x \le L/2$.

Table 3 The permeability of each zone when $a/2 \le \Delta x \le L/2$

Zone	Permeability		
	K_x	K_y	K_z
1	$K_x^1 = \frac{1}{2}K_{box,x} + \frac{1}{2}K_{void,x}^1$	$K_y^1 = \frac{1}{2}K_{box,y} + \frac{1}{2}K_{void,y}^1$	$K_z^1 = \left(\frac{1}{2}\frac{1}{K_{box,z}} + \frac{1}{2}\frac{1}{K_{void,z}^1}\right)^{-1}$
2	$K_x^2 = K_{box,x}$	$K_y^2 = K_{box,y}$	$K_z^2 = K_{box,z}$
3	$K_x^3 = \frac{1}{2}K_{box,x} + \frac{1}{2}K_{void,x}^3$	$K_y^3 = \frac{1}{2}K_{box,y} + \frac{1}{2}K_{void,y}^3$	$K_z^3 = \left(\frac{1}{2}\frac{1}{K_{box,z}} + \frac{1}{2}\frac{1}{K_{void,z}^3}\right)^{-1}$
4	$K_x^4 = K_{box,x}$	$K_y^4 = K_{box,y}$	$K_z^4 = K_{box,z}$
5	$K_x^5 = \frac{1}{2}K_{box,x} + \frac{1}{2}K_{void,x}^5$	$K_y^5 = \frac{1}{2}K_{box,y} + \frac{1}{2}K_{void,y}^5$	$K_z^5 = \left(\frac{1}{2}\frac{1}{K_{box,z}} + \frac{1}{2}\frac{1}{K_{void,z}^5}\right)^{-1}$

2.2 Multilayer Fabric

For multilayer fabrics, the shifting between adjacent layers is independent and random. The permeability of every two-layer fabric is different due to the variety of layer shift. In this paper, every two-layer fabric was regarded as a porous medium with different permeability, as shown in Fig. 6. According to the electrical resistance analogy, the permeability of multilayer fabrics can be written as follows:

$$K_x = \frac{\sum K_x^j \mathrm{h}_\mathrm{j}^{'}}{\sum \mathrm{h}^{'}{}_\mathrm{j}} \tag{38}$$

$$K_y = \frac{\sum K_y^j \mathrm{h}_\mathrm{j}^{'}}{\sum \mathrm{h}^{'}{}_\mathrm{j}} \tag{39}$$

$$K_z = \left(\frac{\sum \frac{\mathrm{h}^{'}{}_\mathrm{j}}{K_z^j}}{\sum \mathrm{h}^{'}{}_\mathrm{j}} \right)^{-1} \tag{40}$$

Where j refers to the number of layer.

Substituting Eqs. (11)–(13) into Eqs. (38)–(40), the permeability of multilayer fabrics can be calculated if every shift between adjacent layers is given. However, layer shift is very difficult to obtain in actual process. When the total thickness is kept constant, the average thickness per layer $\overline{h}$ instead of interlayer distance h', is substituted into Eqs. (38)–(40). The permeability of multilayer fabrics can be rewritten as

$$K_x = \frac{\sum K_x^j}{n} = E\left(K_x^j\right) \tag{41}$$

$$K_y = \frac{\sum K_y^j}{n} = E\left(K_y^j\right) \tag{42}$$

$$K_z = \left(\frac{1}{n}\sum \frac{1}{K_z^j}\right)^{-1} = \left(E\left(\frac{1}{K_z^j}\right)\right)^{-1} \tag{43}$$

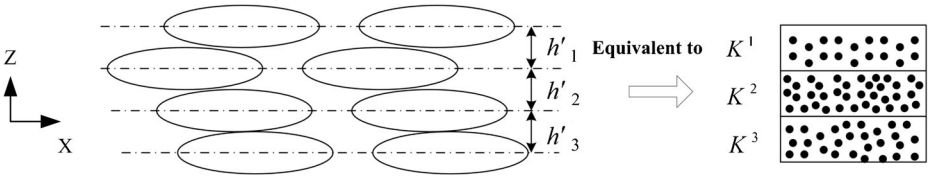

Fig. 6 Equivalent way of the permeability of multilayer unidirectional fabrics

where $E(K_x^j)$, $E(K_y^j)$ and $E\left(\frac{1}{K_z^j}\right)$ are the mathematical expectations of K_x^j, K_y^j and $\frac{1}{K_z^j}$, respectively.

In an effort to acquire statistical characteristics, 1000 uniform random numbers ranging from 0 to $L/2$ acted as the layer shifts. In addition, the uniform random numbers imply that they were randomly selected under the same probability. Using these models, the effect of number of layers was further analyzed.

3 Experiment

3.1 Materials

The unidirectional glass fiber fabric EDW442 supplied by CA.BEN Composites Co., Ltd was used and each bundle contains 2200 fiber filaments with diameter of 16 μm. Laminates were made to measure geometrical parameters of yarns and gaps between yarns in microstructural analyses using the image analysis software Image-Pro Plus. Each parameter was obtained by averaging 10 measurements. The long and short axes of the yarn cross-section are 2.23 mm and 400 μm, respectively. The width of gap between yarns is 350 μm.

The epoxy resin 5015 was used as the model fluid in the permeability runs, with a viscosity of 800 $mPa \cdot s$ at the room temperature.

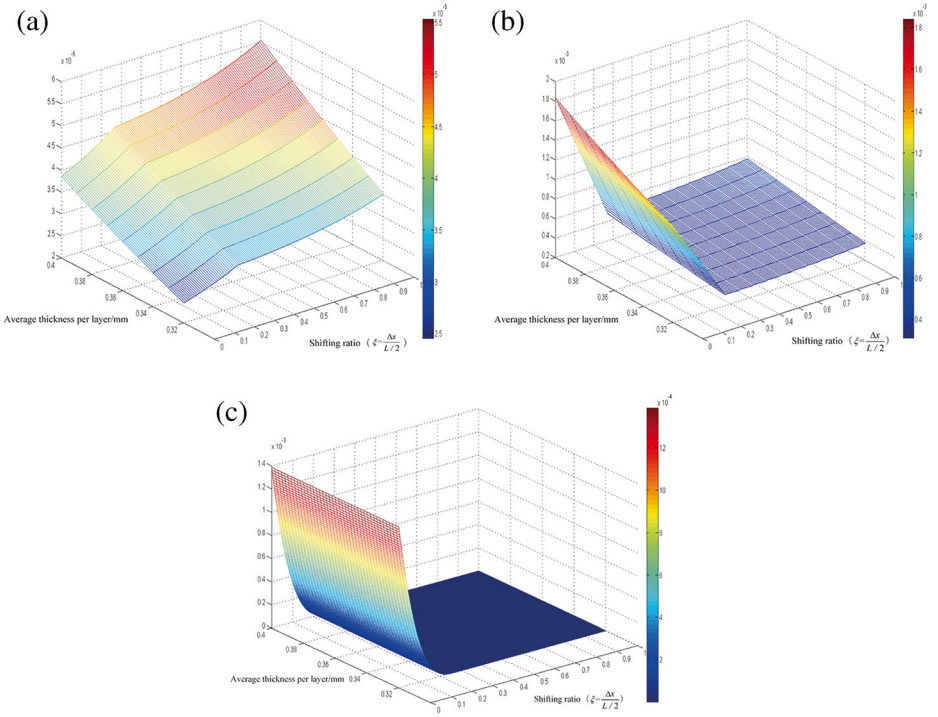

Fig. 7 The change of permeability with respect to average thickness per layer and layer shift for **a** K_x, **b** K_y and **c** K_z

3.2 Experimental Set-up and Procedure

To measure the in-plane permeability, the radial outward flow method was used in an RTM mould with central injection at a constant injection pressure of 0.1 MPa. A video camera was used to record the advancement of the flow during mold filling. The in-plane permeability was then obtained by following Chan and Hwang's method [24]. More detailed explanation is given in the study [20].

To measure the out-of-plane permeability, the fabrics were held by a pair of porous circular walls to fit in a transparent cylindrical flow channel of 60 mm inner diameter. After the samples were compressed to the desired volume fraction and the fluid guided through the cross-section of the cylinder. After the measurements were performed, a linear relationship between pressure drop and flow rate was obtained and then the out-of-plane permeability was calculated. More detailed explanation is given in the study [25].

4 Results and Discussion

4.1 Permeability of a Two-Layer Fabric

Figure 7 shows the analytical results K_x, K_y and K_z of a two-layer fabric with respect to the layer shift and average thickness per layer, respectively. As expected, the

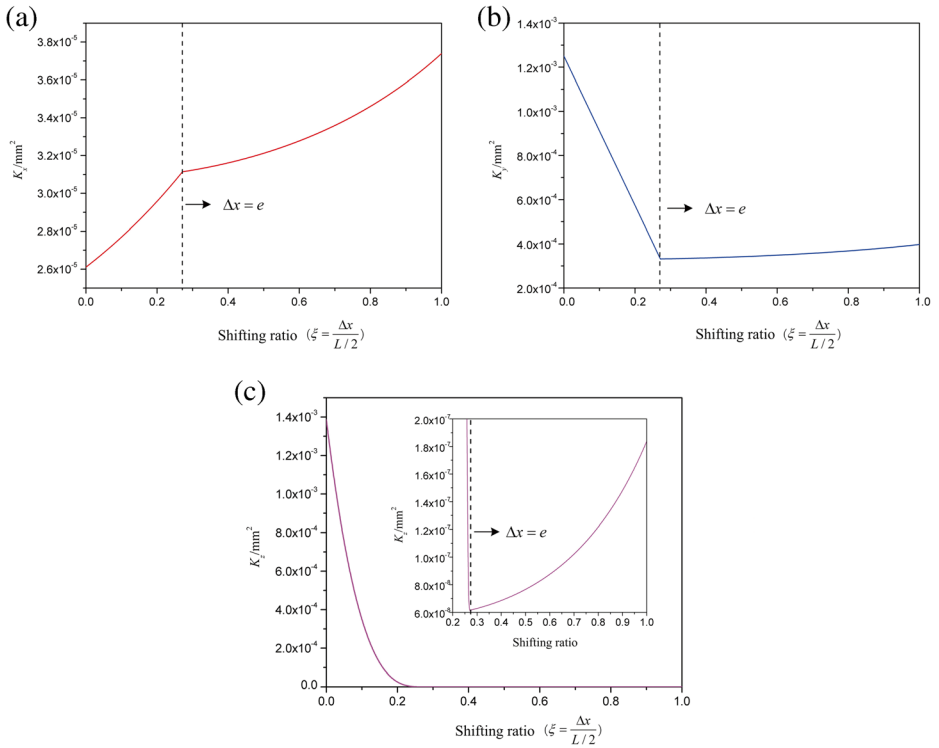

Fig. 8 Permeability as a function of layer shift when average thickness per layer was fixed at 0.35 mm for **a** K_x, **b** K_y and **c** K_z

permeability decreases with the reduction of average thickness per layer due to the increase of fiber volume fraction. However, K_x, K_y and K_z present different variations. To analyze the effect of layer shift, average thickness per layer is fixed at 0.35 mm and the in-plane and out-of-plane permeability as a function of layer shift are shown in Fig. 8.

The permeability K_x increases with increasing the layer shift. K_x reaches minimum when $\Delta x = 0$ and reaches maximum when $\Delta x = L/2$. The ratio of maximum and minimum values is about 1.4. Compared with K_y and K_z influence of layer shift on K_x is weaker as the flow is dominated by compression of the yarns. With the increase of layer shift, the decrease of fiber volume fraction in bundles leads to the increase of permeability of a fiber bundle perpendicular to its axis and finally results in the increase of K_x.

When $0 \le \Delta x \le e$, K_y decreases rapidly with the increase of layer shift as the impregnation properties are dominated by the void spaces in zone 3 in y direction. When $\Delta x = e$, the void space disappears and K_y reaches the minimum value. When $e \le \Delta x \le L/2$, K_y increases slowly with the increase of layer shift. The reason may be that the permeability of a fiber bundle parallel to its axis increases with the decrease of fiber volume fraction of a bundle.

The change of K_z is similar with K_y. When $0 \le \Delta x \le e$, K_z decreases with the increase of layer shift, and reaches the minimum value when $\Delta x = e$. This can also be explained by the variation of void spaces between adjacent yarns which determine the flow in z direction. When

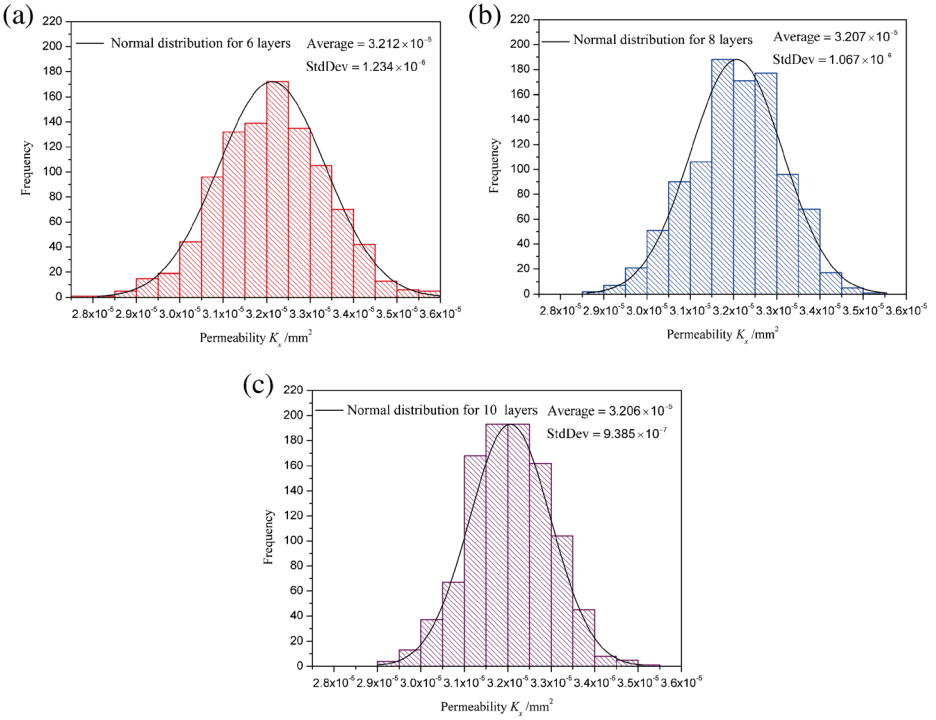

Fig. 9 The distribution of permeability K_x for (**a**) 6 layers (**b**) 8 layers (**c**) 10 layers

$e \le \Delta x \le L/2$, K_z increases slowly as the fiber volume fraction of a bundle decreases with increasing the layer shift.

4.2 Permeability of Multilayer Unidirectional Fabrics

To study the effect of layer shift on in-plane and out-of-plane permeability of multilayer fabrics, the average thickness per layer is fixed at 0.35 mm. The permeability of every two-layer fabric can be calculated by Eqs. (11)–(13) when the layer shift is given randomly in interval [0, L/2]. The permeability of 6, 8 and 10 layers can be regarded as a mixture of 5, 7 and 9 different values as every two-layer fabric is treated as a porous medium, respectively. From a statistical viewpoint, the permeability is analyzed by using the data obtained from 1000 analytical calculations for each of the layer numbers, as shown in Figs. 9, 10, and 11. According to the maximum and minimum values, the distribution of K_x is divided into 17 different intervals and the interval width is $5 \times 10^{-7}\text{mm}^2$. The distribution of K_y is divided into 14 different intervals and the interval width is $5 \times 10^{-5}\text{mm}^2$. The distribution of K_z is divided into 15 different intervals and the interval width is $5 \times 10^{-8}\text{mm}^2$. It can be seen that the histogram of permeability takes the shape close to a normal distribution. The average permeability values of 6, 8 and 10 layers are close to each other, but the standard deviations are different and become smaller with increasing the number of layers resulting that the distributions of permeability become narrow.

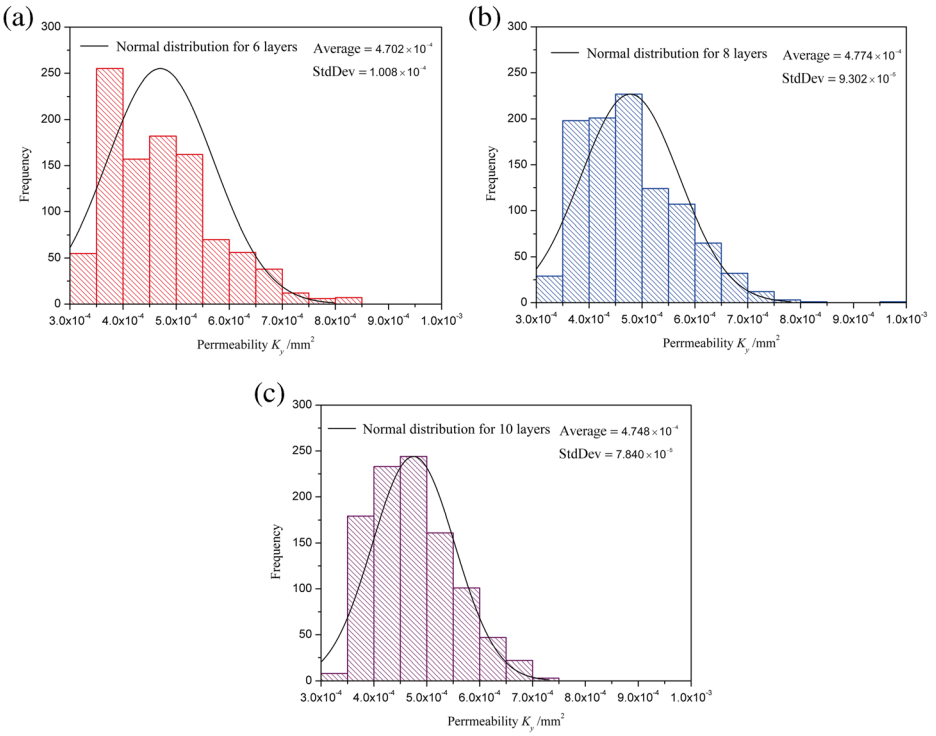

Fig. 10 The distribution of permeability K_y for (**a**) 6 layers (**b**) 8 layers (**c**) 10 layers

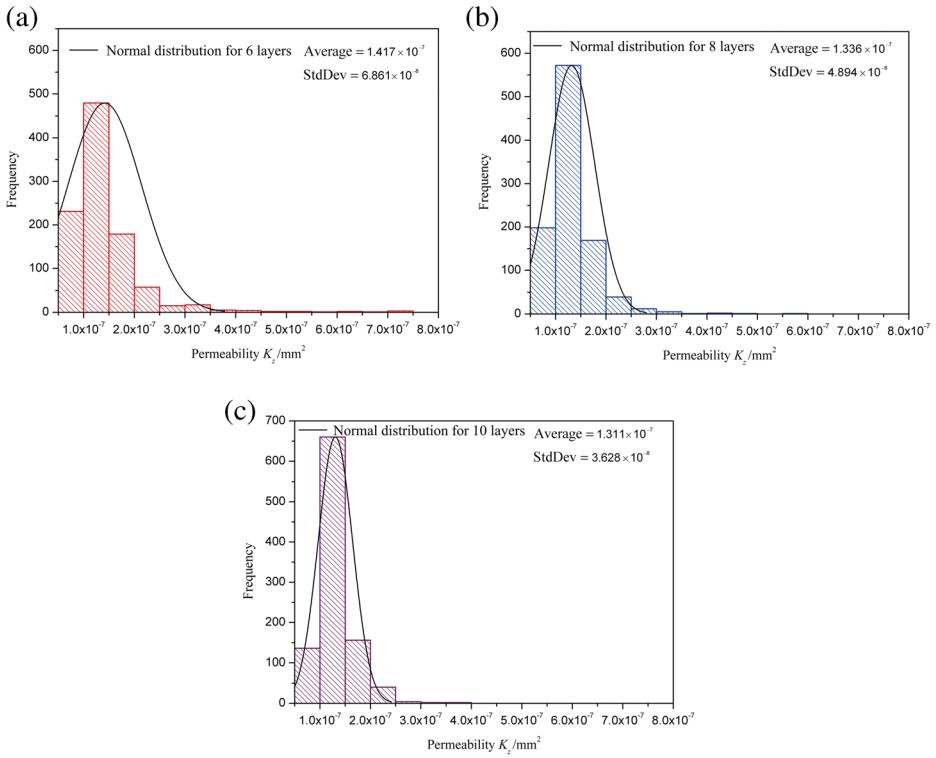

Fig. 11 The distribution of permeability K_z for (**a**) 6 layers (**b**) 8 layers (**c**) 10 layers

To verify the accuracy of permeability models, ten samples were prepared for each of the layer numbers to measure the in-plane and out-of-plane permeability. Then, the experimental results were compared with permeabilities obtained analytically as shown in Fig. 12. Better agreement was found between theoretical and experimental values with increasing the number of layers. For K_x, the relative errors between theoretical and experimental average permeabilities are 21.1 % for 6 layers, 17.9 % for 8 layers and 13.5 % for 10 layers, respectively. Compared with K_x, the relative error of K_y is larger. For K_y, the relative errors between theoretical and experimental average permeabilities are 34.6 % for 6 layers, 23.7 % for 8 layers and 19.1 % for 10 layers, respectively. And theoretical values are generally higher than the experimental values. The reason is that the yarn width has been assumed to be constant in the models when the average thickness per layer changes. Similar trend can be found in papers [26, 27] as the deformation of yarn width due to the compressive force is generally small compared with the deformation of thickness. However, the increase of yarn width, although is small in actual process, can result in the reduction of the width of void space between adjacent yarns, which is one of the main factors affecting the permeability K_y as discussed in Section 4.1. For K_z, the relative errors between theoretical and experimental average permeabilities are 36.4 % for 6 layers, 29.6 % for 8 layers and 22.8 % for 10 layers, respectively. And the theoretical value is generally lower than the experimental values. The reason is that it is difficult to avoid the edge effect. Overall, the

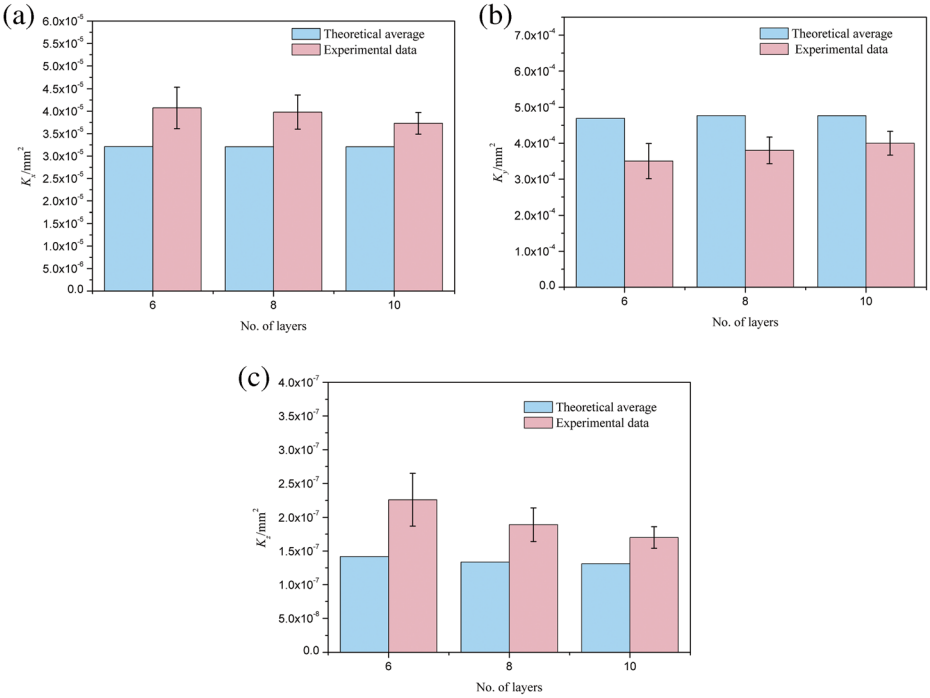

Fig. 12 Comparison of analytically calculated permeability values with experimental data (**a**) for K_x (**b**) for K_y (**c**) for K_z

results of this paper indicate that theoretical predictions agree with the experimental values, and relative error is within an acceptable range.

5 Conclusions

In this paper, models have been presented for the prediction of the in-plane and out-of-plane permeability of multilayer unidirectional fabrics as a function of layer shift to study the effect of nesting. Based on the range of layer shift, three different unit cells were modeled and decomposed into zones of characteristic yarn arrangement, respectively. For each unit cell, a set of equations was derived allowing description of the local permeability of each zone as a function of geometrical yarn parameters. The overall permeability was then modeled as a mixture of permeabilities of different zones with the electrical resistance analogy.

It was found that the permeability K_x increases slowly with the increase of layer shift. K_x reaches minimum when $\Delta x = 0$ and reaches maximum when $\Delta x = L/2$. K_y and K_z decrease rapidly when $0 \le \Delta x \le e$ and increase slightly when $e \le \Delta x \le L/2$ with increasing the layer shift. Both of K_y and K_z reach minimum when $\Delta x = 0$ and reach maximum when $\Delta x = L/2$.

The theoretical statistical results of the permeability of 6-layer, 8-layer and 10-layer unidirectional fabrics indicate that the distribution could be approximated by a normal distribution. Successful permeability predictions in comparison with experimental data were

achieved. The average permeability values are very close while the differences of standard deviations are great among the samples with different layers. With increasing the number of layers, the standard deviation gets smaller, and the distribution of permeability becomes narrow.

Acknowledgments This work was funded by National Nature Science Foundation of China (51573148).

References

1. Deng, C., Jiang, J., Liu, F., et al.: Influence of carbon nanotubes coatings onto carbon fiber by oxidative treatments combined with electrophoretic deposition on interfacial properties of carbon fiber composite. Appl. Surf. Sci. **357**, 1274–1280 (2015)
2. Fang, L.C., Jiang, J., Wang, J., et al.: Non-uniform capillary model for unidirectional fiber bundles considering pore size distribution. J. Reinf. Plast. Compos. **33**(15), 1430–1440 (2014)
3. Demaria, C., Ruiz, E., Trochu, F.: In-plane anisotropic permeability characterization of deformed woven fabrics by unidirectional injection. Part I: experimental results. Polym. Compos. **28**(6), 797–811 (2007)
4. Deng, C., Jiang, J., Liu, F., et al.: Effects of electrophoretically deposited graphene oxide coatings on interfacial properties of carbon fiber composite. J. Mater. Sci. **50**(17), 5886–5892 (2015)
5. Ivanov, D.S., Lomov, S.V.: Compaction behaviour of dense sheared woven preforms: experimental observations and analytical predictions. Compos. Part A **64**(21), 167–176 (2014)
6. Deng, C., Jiang, J., Liu, F., et al.: Influence of graphene oxide coatings on carbon fiber by ultrasonically assisted electrophoretic deposition on its composite interfacial property. Surf. Coat. Technol. **272**, 176–181 (2015)
7. Nguyen, Q.T., Vidal-Sallé, E., Boisse, P., et al.: Mesoscopic scale analyses of textile composite reinforcement compaction. Compos. Part B **44**(1), 231–241 (2013)
8. Deng, C., Jiang, J., Liu, F., et al.: Influence of surface properties of graphene oxide/carbon fiber hybrid fiber by oxidative treatments combined with electrophoretic deposition. Surf. Interface Anal. **48**, 212–217 (2016)
9. Kruckenberg, T., Lin, Y., Paton, R., et al.: Static and vibration compaction and microstructure analysis on plain-woven textile fabrics. Compos. Part A **39**(3), 488–502 (2008)
10. Hoes, K., Dinescu, D., Sol, H., Parnas, R., Lomov, S.V.: Study of nesting induced scatter of permeability values in layered reinforcement fabrics. Compos. Part A **35**(12), 1407–1418 (2004)
11. Dungan, F.D., Senoguz, M.T., Sastry, A.M., Faillaci, D.A.: Simulations and experiments on low-pressure permeation of fabrics: Part I - 3D modeling of unbalanced fabric. J. Compos. Mater. **35**(14), 1250–1284 (2001)
12. Senoguz, M.T., Dungan, F.D., Sastry, A.M., Klamo, J.T.: Simulations and experiments on low-pressure permeation of fabrics: Part II - The variable gap model and prediction of permeability. J. Compos. Mater. **35**(14), 1285–1322 (2001)
13. Endruweit, A., McGregor, P., Long, A.C., Johnson, M.S.: Influence of the fabric architecture on the variations in experimentally determined in-plane permeability values. Compos. Sci. Technol. **66**(11–12), 1778–1792 (2006)
14. Endruweit, A., Long, A.C.: A model for the in-plane permeability of triaxially braided reinforcements. Compos. Part A **42**(2), 165–172 (2011)
15. Grujicic, M., Chittajallu, K.M., Walsh, S.: Effect of shear, compaction and nesting on permeability of the orthogonal plain-weave fabric performs. Mater. Chem. Phys. **86**(2), 358–369 (2004)
16. Grujicic, M., Chittajallu, K.M., Walsh, S.: Lattice Boltzmann method based computation of the permeability of the orthogonal plain-weave fabric preforms. J. Mater. Sci. **41**(23), 7989–8000 (2006)
17. Lekakou, C., Edwards, S., Bell, G., Amico, S.C.: Computer modelling for the prediction of the in-plane permeability of non-crimp stitch bonded fabrics. Compos. Part A **37**(6), 820–825 (2006)
18. Tran, T., Comas-Cardona, S., Abriak, N.E., et al.: Unified microporomechanical approach for mechanical behavior and permeability of misaligned unidirectional fiber reinforcement. Compos. Sci. Technol. **70**(9), 1410–1418 (2010)
19. Fang, L.C., Jiang, J., Wang, J., et al.: Effect of nesting on the out-of-plane permeability of unidirectional fabrics in resin transfer molding. Appl. Compos. Mater. **22**(3), 1–19 (2015)
20. Fang, L.C., Jiang, J., Wang, J., et al.: The effect of nesting on the in-plane permeability of unidirectional fabrics in resin transfer molding. Polym. Compos. (2015). doi:10.1002/pc.23342

21. Zeng, X., Endruweit, A., Brown, L.P., Long, A.C.: Numerical prediction of in-plane permeability for multilayer woven fabrics with manufacture-induced deformation. Compos A: Appli Sci Manuf **77**:266–274 (2015)
22. Ni, J., Zhao, Y., Lee, L.J., Nakamura, S.: Analysis of two-regional flow in liquid composite molding. Polym. Compos. **18**(2), 254–269 (1997)
23. Gebart, B.R.: Permeability of unidirectional reinforcements for RTM. J. Compos. Mater. **26**(8), 1100–1133 (1992)
24. Chan, A.W., Hwang, S.T.: Anisotropic in-plane permeability of fabric media. Polym. Eng. Sci. **31**, 1233–1239 (1991)
25. Fang, L.C., Jiang, J., Wang, J., et al.: Effect of layer shift on the out-of-plane permeability of 0 / 90 noncrimp fabrics[J]. J. Reinf. Plast. Compos. **33**(22), 2073–2094 (2014)
26. Chen, B.X., Chou, T.W.: Compaction of woven-fabric preforms in liquid composite molding processes: single-layer deformation. Compos. Sci. Technol. **59**(10), 1519–1526 (1999)
27. Chen, Z.R., Ye, L., Kruckenberg, T.: A Micromechanical compaction model for woven fabric preforms. Part I: single layer. Compos. Sci. Technol. **66**, 3254–3262 (2006)